Trans Indian Inst Met
DOI 10.1007/s12666-016-0935-3

TECHNICAL PAPER

Hot Rolling of a Non-heat Treatable Aluminum Alloy: Thermo-Mechanical and Microstructure Evolution Model

A. B. Nellippallil[1] · P. S. De[2] · A. Gupta[3] · S. Goyal[4] · A. K. Singh[5]

Received: 17 May 2016 / Accepted: 18 July 2016

Abstract A transient thermo-mechanically coupled Finite Element Method based model for single pass hot rolling of AA 5083 aluminum alloy is developed. The formulation is based on thermo-viscoplastic behavior expressed by the Perzyna constitutive equation and rolling under plane-strain conditions. The finite element model is integrated with a microstructural model where dynamic recrystallization through particle stimulated nucleation and static recrystallization is considered. The dynamic recrystallization model is an adoption of discontinuous dynamic recrystallization model while static recrystallization model is based on Avrami equation. The simulation results indicate that accurate estimates of constitutive behavior of the alloy, efficiency of conversion of plastic deformation to heat, and heat transfer at the roll/metal interface are critical for precise hot rolling model.

Keywords Hot rolling · AA 5083 aluminum alloy · Finite Element Method · Dynamic recrystallization · Static recrystallization

✉ P. S. De
parthasarathi.de@iitbbs.ac.in

[1] University of Oklahoma, Norman, OK, USA

[2] SMMME, IIT Bhubaneswar, Room 602, A1 Block, Toshali Bhavan, Bhubaneswar 751007, India

[3] TRDDC-TCS Innovation Center, TCS Ltd., Pune, India

[4] CEAT Limited, Vadodara, India

[5] Department of Materials Science and Engineering, IIT Kanpur, Kanpur, India

1 Introduction

Hot rolling is a thermo-mechanical process of plastically deforming a wrought metal to a desired dimension and mechanical property. Thus, an appropriate selection of the process variables (i.e. temperature, rate of heating/cooling, strain, strain rate) during hot rolling is critical to achieve the optimum physical properties. Experimental approach to optimize thermo-mechanical processing is very costly as well as time consuming, forcing researchers to increasingly focus on simulation techniques [1–16]. Nonetheless, the strongly coupled multi-physics nature of such processes makes it one of the challenging simulation problems in materials processing. The present work consists of two parts. The first part comprises of a two dimensional FEM based model for single pass hot rolling of AA 5083 aluminum alloy to predict the temperature, strain and strain rate variation during rolling. The second part comprises of a microstructure evolution model with sub-models for (1) dynamic recrystallization and (2) static recrystallization, to predict its evolution during rolling. The thermo-mechanical data generated from the FEM model is used as an input to the microstructure model. The microstructure and the temperature history data predicted from this, hot rolling Through Process Model (TPM), is then validated with the experimental works of Wells et al. [8].

A survey of hot rolling simulation literature reveals that majority of the published research is in the area of steel. Reports on TPM of Aluminum alloys are comparatively less [8–12] which is in part, a result of the complexities arising in the heat transfer process (boundary condition) from the work-piece to the roll. In Table 1, the heat transfer coefficient for steel work-piece/roll and aluminum work-piece/roll is presented. The heat transfer coefficient used for Al alloy simulations is observed to be lower than that

Published online: 30 July 2016

Table 1 Heat transfer coefficient values used between roll and work-piece (steel/aluminum alloys) during hot rolling

Work-piece material	Heat transfer coefficient (kW/m^2 K)	References
Steel	50	[14]
Steel	30	[15]
Aluminum alloy	18	[12]
Aluminum alloy	11	[16]
Aluminum alloy	25	[17]

assumed during steel rolling [12–16]. Apparently, this is inconsistent with the fact that Al alloys are at least 3–4 times more conductive than steel. On the other hand, Wells and co-workers assumed a high heat transfer coefficient values between 200 and 450 kW/m^2 K [8, 9] which is an order of magnitude higher than other works [12, 15, 16]. Thus, an ambiguity exists with respect to the heat transfer coefficient values. The work roll temperature during rolling simulation is another aspect which is dealt with tentatively in most published literature [8, 9, 12–16]. Wells et al. [8, 9] dealt this aspect as a boundary condition where the roll is assumed to behave adiabatically at a distance of 5 cm from the surface while Shahani et al. [16], used a distance of 10 cm from surface. No specific reason for the choice has been given by these researchers. Moreover, use of boundary conditions which are experimentally unverifiable, makes it unrealistic to compare the simulation results with practical experiments. The heat transfer coefficient and the roll temperature influences the heat flow from the work-piece during hot rolling and incorrect assumptions would result in an erroneous estimate of the final microstructure. Similarly, the simulation of microstructure evolution has its own share of inconsistencies. Thus, during hot working, Al alloys can exhibit dynamic recovery, recrystallization or even a combination of both depending on the alloying elements used [17]. The dynamic recrystallization process can again be of discontinuous or continuous type, where processes like particle stimulated nucleation further complicates the recrystallization process. Thus, aluminum based alloys require a more complex physical based approach to model the microstructure evolution. Internal variable based models for dynamic recovery or recrystallization have already been proposed in literature [18, 19]. But, the extension of the same to particle stimulated nucleation has not been examined.

The principal aim in this work is to implement a TPM for hot rolling of AA 5083 alloy under warm rolling conditions where particle stimulated nucleation is expected to occur. The simulated results are compared with experimental data obtained from literature. In the next section, the modeling details have been discussed in more details.

2 Model Details

In this work the thermo-viscoplastic process during hot rolling has been modeled using a commercial FEM software ANSYS. The rolls have been modeled as a rigid body which deforms an AA 5083 aluminum alloy strip under plain strain conditions [9]. The temporal change in temperature, strain and strain rate obtained from the simulation model during rolling have been used to determine the final microstructure. The next sub-section discusses the finite element model for rolling in more details.

2.1 Finite Element Model

The single pass hot rolling model developed in this work uses a coupled approach, where the thermal and structural loads are applied and solved simultaneously. The mathematical model for the same is represented as [20],

$$\begin{bmatrix} 0 & 0 \\ 0 & C^t \end{bmatrix} \begin{pmatrix} \{\dot{u}\} \\ \{\dot{T}\} \end{pmatrix} + \begin{bmatrix} [K] & 0 \\ 0 & [K^t] \end{bmatrix} \begin{pmatrix} \{u\} \\ \{T\} \end{pmatrix} = \begin{pmatrix} \{F\} \\ \{Q\} \end{pmatrix} \tag{1}$$

where $\{\dot{T}\}$ is the vector of the temperature rate, $\{T\}$ is the vector of the temperatures, $\{F\}$is the vector of structural load, $\{Q\}$ is the vector of the total heat flow (given by the sum of the contributions due to convection at the surface and the heat generated internally), $\{\dot{u}\}$ is the vector of the velocity, {u} is the vector of the displacements, $[K]$ is the stiffness matrix, $[K^t]$ is the thermal conductivity matrix and $[C^t]$ is the specific heat matrix. The governing equation for the thermal flow is represented as,

$$k\nabla^2 T + \dot{q} = pc\frac{\partial T}{\partial t} \tag{2}$$

where p (in kg/m^3) is the density, c (in J kg^{-1} $°C^{-1}$) is the specific heat capacity, k (in W m^{-1} $°C^{-1}$) is the thermal conductivity and $\dot{q}$ (in W m^{-3}) is the heat generation term. The heat generation $(\dot{q})$ is considered to be both volumetric (due to plastic deformation) and due to friction at the roll/strip interface [21]. The transformation of deformation energy to heat $\dot{q}_{pl}$ is calculated as [2]

$$\dot{q}_{pl} = \eta\bar{\sigma}\bar{\dot{\varepsilon}} \tag{3}$$

where $\bar{\sigma}$ (in MPa) is the effective flow stress, $\bar{\dot{\varepsilon}}$ (in s^{-1}) is the effective strain rate and η the conversion efficiency of plastic deformation energy to heat is assumed to be 0.9 [22, 23]. The frictional heat generation (q_{fric}) occurring at the roll/strip interface is given as [3],

$$q_{fric} = \tau_{crit} v \tag{4}$$

where v is the sliding velocity and τ_{crit} is the shear stress which is related to the coefficient of friction by,

$$\tau_{crit} = \mu P \tag{5}$$

where P is the normal force acting on the strip and μ is coefficient of friction assumed to be 0.3 [8].

The strip geometry is modeled using the 2D 8-node coupled field element, PLANE223, while the contact between the rigid roll and the strip is modeled using a 2D 3-node surface to surface contact element, CONTA172. In a practical rolling condition, the contact between roll and strip is imperfect, which results in a temperature discontinuity at the contact interface. This imperfection is incorporated in the model by using a thermal contact conductance [20]. The geometrical model for strip and roll is identical to the experimental work of Wells et al. [8, 9, 24] where an initial strip length and thickness of 50 and 9.6 mm respectively at an initial temperature of 315 °C have been used. The rolling is performed with a roll of diameter 400 mm at an average strain rate $\bar{\dot{\varepsilon}}$ of 11.5 s^{-1} and a total strain (single pass) of 0.26 [8]. The rolling speed is calculated using the analytical equation [25]

$$\bar{\dot{\varepsilon}} = \frac{2\pi R^* N^*}{60\sqrt{R^* \Delta H}} \ln \frac{H_o}{H_f} \tag{6}$$

where R^* is the roll radius, N^* is the roll speed in RPM (revolution per minute) and ΔH is the difference in initial (H_o) and final strip thickness (H_f). A summary flowchart for FEM model is provided in Fig. 1.

The visco-plastic behavior of AA 5083 at the rolling temperatures is modeled using the Perzyna model given as [26],

$$\sigma = \left[1 + \left(\frac{\dot{\varepsilon}^{pl}}{\gamma(T)}\right)^{m(T)}\right] \sigma_O\left(\varepsilon^{pl}, T\right) \tag{7}$$

where σ is the dynamic yield stress, expressed as a function of plastic strain rate $\dot{\varepsilon}^{pl}$, the material viscosity parameter $\gamma(T)$, strain rate hardening parameter $m(T)$, and the static yield stress σ_O. The uniaxial static behavior of the material is assumed to be bilinear isotropic where the initial slope of the stress–strain curve is defined by the Young's modulus (70 GPa) and is assumed to be independent of temperature. Above the yield stress the plastic strain is assumed to depend on the tangent modulus defined by the slope of the plastic curve and is a function of temperature. In Tables 2 and 3, the different material constants used in the FEM model are presented.

In any modeling effort, the choice of boundary conditions are critical. In the given problem, the thermal boundary conditions used are as follows [16]:

1. At the centerline of the strip, a symmetry condition is assumed, i.e.

$$-K_{strip} \frac{\partial T}{\partial y} = 0 \quad at\ t > 0, \quad y = 0 \tag{8}$$

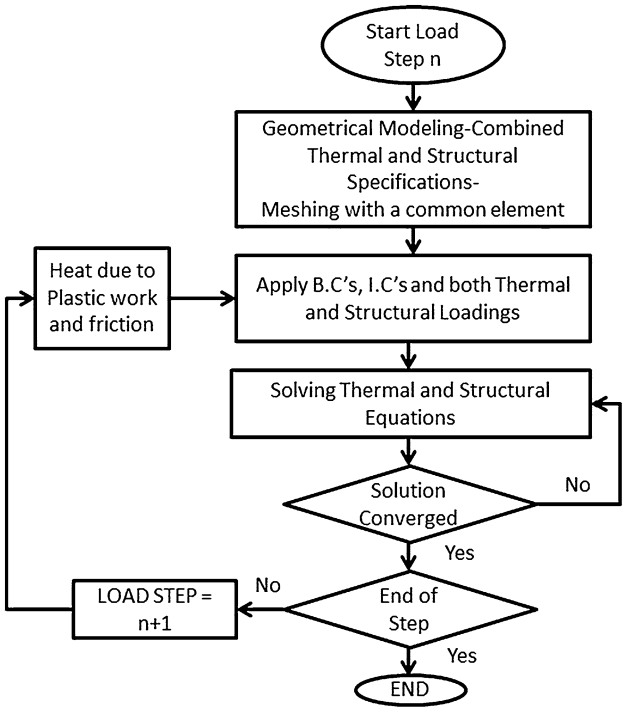

Fig. 1 Flow chart of finite element model for hot rolling process

Table 2 The thermo-physical properties of AA 5083 alloy used in the FEM model [8]

Temperature (°C)	Heat capacity (J kg^{-1} K^{-1})	Thermal conductivity (W m^{-1} K^{-1})
14	930	143.4
280	990	167.1
306	1010	170.2
410	1050	174.1
505	1160	185.4

Table 3 The yield stress and tangent modulus variation for AA 5083 [32]

Temperature (°C)	Yield stress (MPa)	Tangent modulus (GPa)
100	145	1.61
283	62.3	1.31
350	36.5	1.15
400	26.5	1.04
450	21.1	0.85
500	16	0.77

indicating a symmetric heat withdrawal irrespective of the roll position. The simulation is therefore conducted on only one half of the strip.

2. At the interface between the strip and the roll surface, the heat transfer is assumed as,

$$q_{strip} = -q_{roll} = h\left(T_{strip} - T_{roll}\right) \quad at\ t > 0 \tag{9}$$

The interface heat transfer coefficient h between the work roll and the strip is considered to be a function of interface pressure (P^*) [27–30] and is calculated using the relationship

$$h = 11.394P^* + 137.53 \tag{10}$$

where P^* is obtained from the experimentally measured roll load [8]. Substituting the value in Eq. (10) yields a heat transfer coefficient value of nearly 450×10^3 $Wm^{-2}K^{-1}$. The temperature of the roll in contact with the strip is assumed to be 90 °C. The heat transfer coefficient value for the air exposed portion of the strip is assumed to be 10 W m^{-2} K^{-1} [8] and the ambient temperature is assumed to be 45 °C [31].

2.2 Microstructure Model

The AA 5083 alloy used in this work is a non-heat treatable alloy which is expected to recrystallize (dynamic/static) during hot rolling [17]. For a high stacking fault energy metal like Al, discontinuous DRX (dDRX) is observed only at high purities [17]. In AA 5083, the presence of $AlMn_6$ dispersoid particles with sizes ranging from 0.2 to 2 μm result in alternative DRX mechanism [17]. Particles with size >1 μm are known to cause particle stimulated nucleation (PSN) type of DRX (henceforth PSN-DRX) [17, 33]. This occurs at warm rolling temperatures where the strain rate is greater than 1 s^{-1} [17]. The present work therefore proposes a PSN-DRX model for AA 5083 where a modified version of the physically based internal variable method for meso-scale dDRX [18, 25] is used. During the post rolling period or in between the roll strands, SRX is considered and is modeled using the Avrami equation [31]. In the next subsections, the details of the different recrystallization models used have been discussed.

2.2.1 Dynamic Recrystallization Model

In the PSN-DRX model proposed in this work, average dislocation density is assumed as the controlling internal microstructural variable. The recrystallized fraction is computed as a function of the average dislocation density that varies during the hot rolling process. The present model is a simplified version of the original model developed by Sandström and Lagneborg [19] where dislocation density distribution is replaced by an average dislocation density (ρ) [25, 34, 35]. The temporal evolution of $\rho(t)$ is expressed as a function of strain hardening, recovery and recrystallization,

$$\frac{d\rho(t)}{dt} = \frac{\dot{\varepsilon}}{bl} - \bar{k}\dot{\varepsilon}\rho(t) - \frac{\bar{m}\gamma^*}{D}\vartheta\bar{\tau}\rho(t)^r\bar{R}[\rho(t) - \rho(cr)] \tag{11}$$

where the first term on the right hand side is the contribution to ρ from strain hardening and is a function of $\dot{\varepsilon}$ the instantaneous strain rate, b the Burger's vector and l the mean free path of dislocation movement. The second term expresses the dislocation density reduction due to recovery which is a function of strain rate, instantaneous dislocation density (t) and $\bar{k}$ is the self-diffusion coefficient. The third term indicates the reduction in dislocation density due to recrystallization, where $\bar{m}$ is mobility of high angle boundary, γ^* is the fraction of mobile high angle boundary, D is the grain size, $\bar{\tau}$ is the energy per unit length of dislocation, ϑ and r being constants. The recrystallization process is active when ρ is above a critical value and is controlled by the function $\bar{R}[\rho(t) - \rho(cr)]$, which is defined as [36],

$$\bar{R}[\rho(t) - \rho(cr)] = \begin{cases} 0 & \rho < \rho_{cr} \\ \rho(t - t_{cr}) & \rho \geq \rho_{cr} \end{cases} \tag{12}$$

The above recrystallization process occurs due to mobile high angle boundary movement where the mobile high angle boundary fraction (γ^*) is expressed as [25],

$$\gamma^* = [1 - \exp(-X)](1 - X)\left(\frac{\rho}{\rho_{cr}}\right)^{q_1} \tag{13}$$

where q_1 is a constant and ρ_{cr} is the critical dislocation density required for recrystallization expressed as [25]

$$\rho_{cr} = \frac{8\sigma_g}{\bar{\tau}l}. \tag{14}$$

where σ_g is the energy of high angle grain boundary, and $\bar{\tau}$ and l are the variables as mentioned previously. The variable X in Eq. (13) is the fraction recrystalzed at the given time instance such that [25]

$$\frac{dX}{dt} = \frac{\vartheta\gamma^*}{D}\bar{m}\bar{\tau}\rho_i \tag{15}$$

where ϑ is a constant with value of 6 [19], while all other variables are as mentioned earlier. The grain boundary mobility $\bar{m}$. which characterizes the ability of mobile high angle boundaries to move is given as [25]:

$$\bar{m} = \bar{m}_o exp\left(\frac{-Q_m}{RT}\right). \tag{16}$$

where $\bar{m}_o$ is the constant of mobility, Q_m is the activation energy for grain boundary movement and R is the gas constant. The self-diffusion coefficient $\bar{k}$. is given as [33],

$$\bar{k} = \bar{k}_o \exp\left(\frac{-Q_s}{RT_k}\right) \tag{17}$$

where $\bar{k}_o$ is a constant and Q_s is the activation energy for self-diffusion. The mean free path (l) for mobile dislocation

movement (Eqs. 11, 14) is considered to be equal to the subgrain size (d_s) and is given as [17]

$$l^{-1} = d_s^{-1} = a_1 + b_1 \log Z \tag{18}$$

wherere a_1 (−0.55E6) [17] and b_1 (0.044E6) [17] are constants while, Z is the Zener Hollomon parameter given as

$$Z = \dot{\varepsilon} \exp\left(\frac{-Q_D}{RT}\right) \tag{19}$$

where $\dot{\varepsilon}$ and T are the strain rate and temperature during deformation (obtained from the FEM model) and Q_D is the activation energy for deformation. Apart from the evolution of dislocation density, the grain size also evolves with time. The velocity of grain boundary movement is considered to be a function of (a) the grain boundary curvature which is always positive and (b) reduction in grain size due to nucleation of new grains at the old grain boundaries. The change in grain size (D) is therefore given as [25],

$$\frac{dD}{dt} = \frac{\bar{m}\sigma_g}{D} - D\frac{dX}{dt}\ln N \tag{20}$$

where N is the number of possible nucleation sites on a given grain and is given by the expression,

$$N = Constant \tag{21}$$

In this work, the value of N is assumed to be $\sim$2 particles/mm^2 and is based on the distributions reported in literature for similar commercial Al alloys [37]. This value of N is assumed to remain unchanged with each rolling pass. Using the above Eqs. (11–21) along with the data for temporal evolution of temperature (obtained from the FEM model) the extent of dynamic recrystallization during rolling is predicted. The values of different constants used in the microstructural model are summarized in Table 4.

2.2.2 Static Recrystallization Model

The model for static recrystallization is based on the Avrami equation given as [31]

$$X = 1 - exp\left(-0.693\left(\frac{t}{t_{0.5}}\right)^n\right) \tag{22}$$

where, n is a constant, t is the time elapsed after deformation and $t_{0.5}$ is the time required for 50 % recrystallization given as [31],

$$t_{0.5} = Ad_0^a f(\varepsilon) Z^{c_1} \times exp\left(\frac{Q_{Rx}}{RT_a}\right) \tag{23}$$

where, A, a, c_1 are constants and T_a is the static recrystallization temperature. The Eqs. 22 and 23 are used for isothermal conditions only. For cases where the temperature changes with time, the variable 't' is replaced by a temperature compensated time W, expressed as [31],

$$W = \sum t_i exp\left(\frac{-Q_{Rx}}{RT_i}\right) \tag{24}$$

and $t_{0.5}$ is replaced by $W_{0.5}$ given as,

$$W_{0.5} = Ad_o^a f(\varepsilon)\bar{Z}^{c_1} \tag{25}$$

where, $\bar{Z}$ is calculated using an averaging process [31].

Table 4 The list of different material constants used in the microstructure model and the numerical values thereof

Parameters used	Values (units) [ref.]
A	2.7 × E−5 [31]
d_0	77 (μm) [8]
a	2.45 [31]
f(ε)	$(9.75 + 3.82\bar{\varepsilon}^2)^{-1}$[31]
c_1	−0.58 [31]
N	2 [37]
Q_{Rx}	183,000 (J/mol) [31]
G (shear modulus)	26.4 (GPa) [38]
b	0.286 (nm) [38]
Q_d	175,000 (J/mol) [8]
$\bar{k}_o$	170 (mm^2 s^{-1}) [33]
Q_s	142,000 (J/mol) [33]
σ_g	0.324 (J/m^2) [39]
$\bar{m}$	10^{-12} (m^4 J s^{-1}) [40]

3 Results

In this section, the temperature, strain and microstructural evolution predicted from the hot rolling model described above is presented.

3.1 Temperature Distribution During Hot Rolling

The predicted temperature of the deformed strip indicates that the temperature increases at the strip center but is reversed at the surface (Fig. 2) indicating heat dissipation from strip surface. Figures 3 and 4 presents the temperature profile predicted at the centerline and surface of the strip. Depending on the material model used, the predicted values differ from the experimental data [8], the implication of which is discussed later.

3.2 Strain During Hot Rolling

The von Mises equivalent strain predicted through the thickness of the strip is compared with the actual measurements reported by Wells et al. [8] in Fig. 5. The

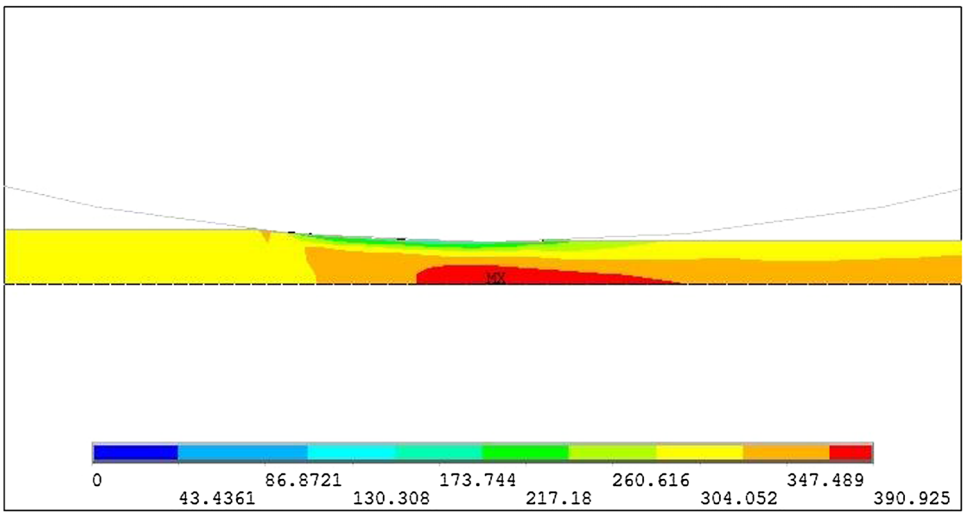

Fig. 2 Simulated temperature profile along the strip during hot rolling

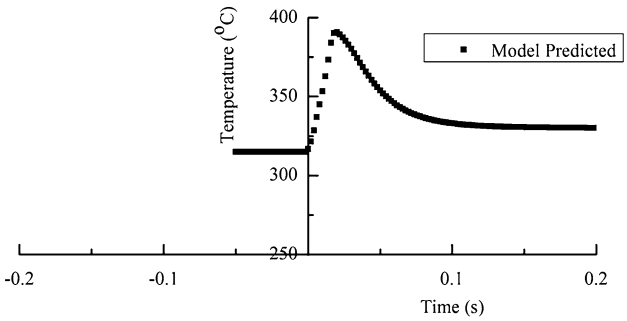

Fig. 3 Temperature profile predicted at the centerline of the strip

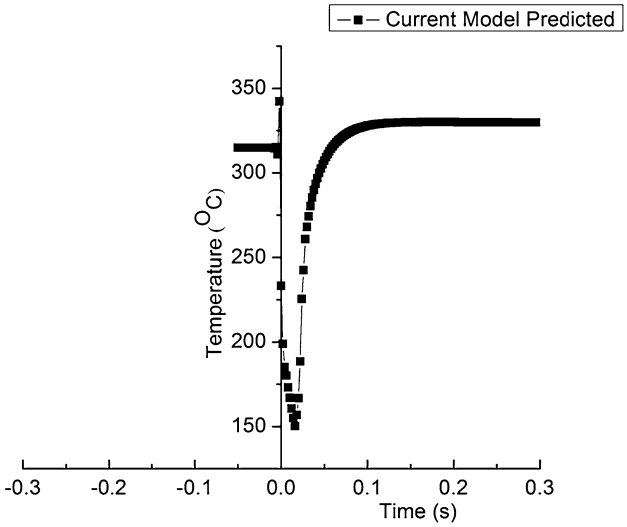

Fig. 4 Temperature profile predicted at the surface of the strip

computed values are less compared to the measured values but are within the limits of variance for the experimental data [8].

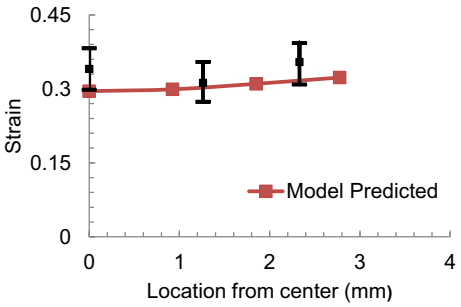

Fig. 5 Comparison of predicted strain with experiment (*black squares* with *error bars*)

3.3 Dynamic Recrystallization During Hot Rolling

Analysis of dynamic recrystallization indicates that for a node along the strip surface, a nominal fraction is recrystallized (Fig. 6). The grain size is also similar to the original (Fig. 7). The temporal change in dislocation density and the critical density of dislocation required to recrystallize is presented in Fig. 8. The dislocation density is observed to increase beyond the critical density for recrystallization only for a very short time period at the point of exit from the rolls.

3.4 Static Recrystallization After Rolling

The static recrystallization after rolling predicted using the Johnson–Mehl–Avrami–Kolmogorov (JMAK) equation shows a variation in fraction recrystallized from the center to the strip surface (Fig. 9). The calculation is performed using the $t_{0.5}$ value used in Ref. [8]. The results indicate that static recrystallization is higher at the surface compared to the center.

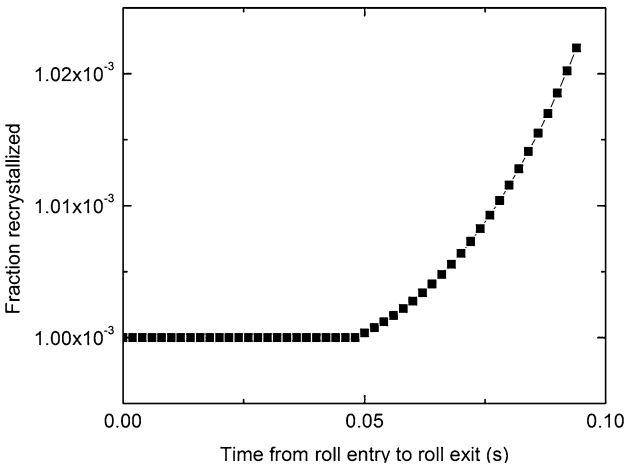

Fig. 6 Fraction dynamic recrystallized as predicted by internal variable method. The DRX effect is negligible and is on expected lines since dynamic recovery effect is more viable

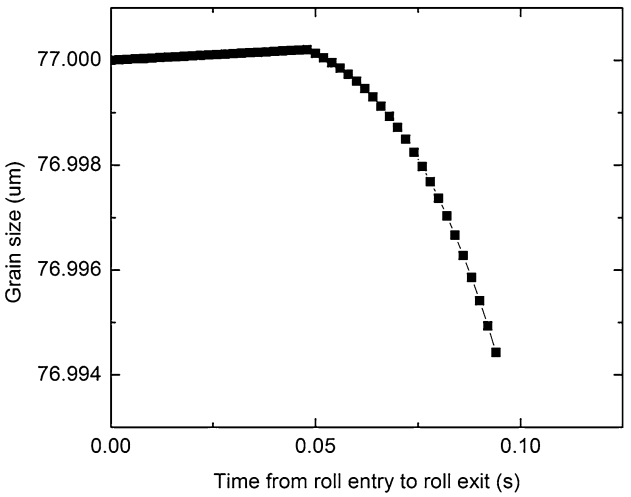

Fig. 7 Grain size evolution during rolling predicted by the internal variable method

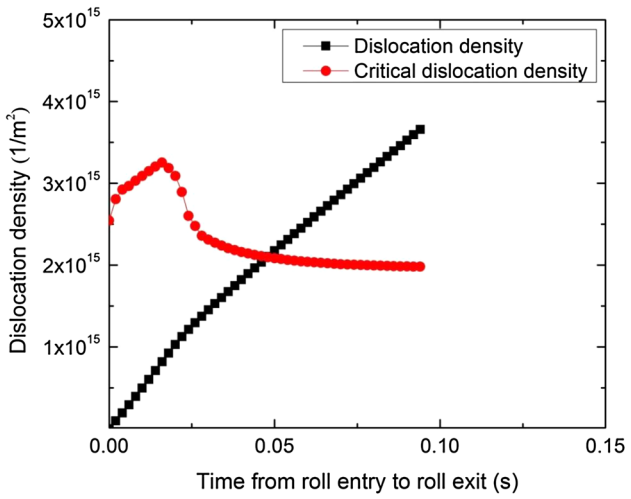

Fig. 8 Evolution of ρ and ρ_{cr}. with time as predicted by the internal variable method

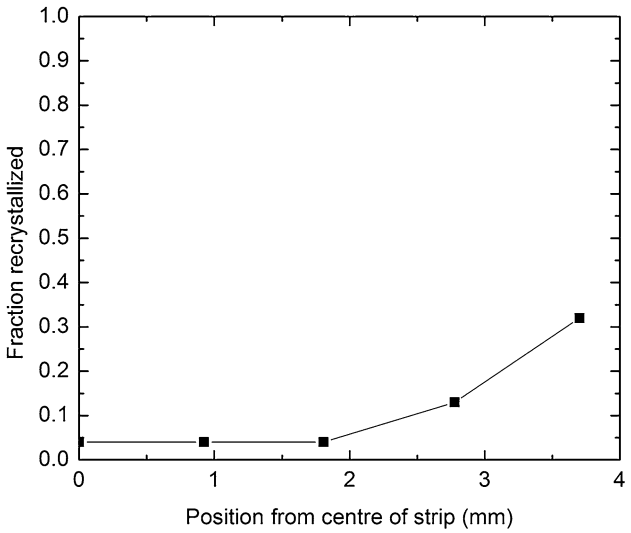

Fig. 9 Percentage recrystallization through thickness of specimen as predicted by the Avrami model used in this work

4 Discussion

The predicted temperature, strain and fraction recrystallized at the surface and center of the strip are similar in trend with the experimentally measured data. The extant deviations are due to sensitivity of thermo-mechanical simulation to modeling parameters as are discussed below.

4.1 Effect of Constitutive Equations and Friction on Temperature Prediction

The viscoplastic flow equation adopted plays a critical role in predicting the temperature. Depending on the dynamic flow stress, the work done during rolling and the deformation heat generated varies significantly. As an example, the flow formulation introduced by Hensel and Spittel depends on equivalent strain, strain rate, temperature and is given as [41]

$$\bar{\sigma} = Se^{j_1 T}\bar{\varepsilon}^{j_2}\dot{\bar{\varepsilon}}^{j_3}e^{j_4/\bar{\varepsilon}} \tag{26}$$

where, S, j_1, j_2, j_3, j_4 are material constants. For AA 5083 the values are 953.655 MPa, −0.00524, 0.01407, 0.11 and −0.00913 respectively [31]. In comparison to the Perzyna constitutive equation used in this work, the Hensel and Spittel equation [31] for AA 5083 shows a positive deviation of $\sim$ 50 MPa in average flow stress. The difference is negative in the low strain region and becomes positive at higher strains (Fig. 10). An additional influence of strain on flow stress in the Perzyna equation is with respect to the

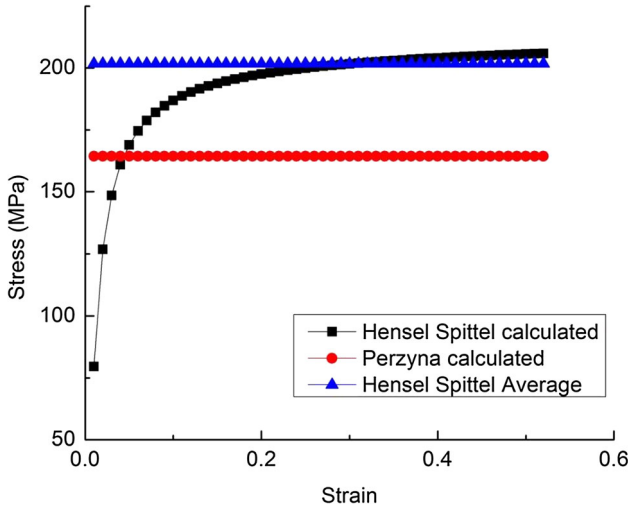

Fig. 10 Comparison of Hensel-Spittel behavior with Perzyna behavior at a temperature of 283 °C and strain rate of 0.81 s^{-1} for AA 5083

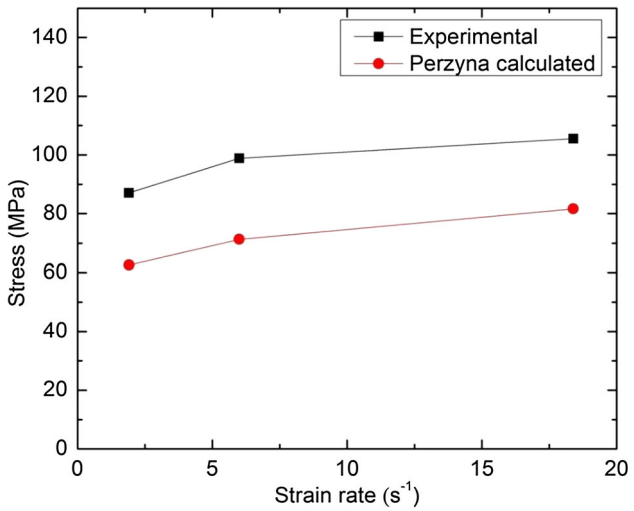

Fig. 11 Variation of dynamic flow stress as predicted by Perzyna equation compared with experimental data for a temperature of 450 °C

effect of static yield stress. In Fig. 11, the experimentally measured stress strain rate data for AA 5083 [42] at 450 °C, is plotted and compared with the Perzyna equation values used in this work. The results indicate that the experimental stress plots with strain rate for different temperature deviate considerably from the Perzyna prediction. In fact, the simpler bilinear isotropic model for plasticity predicts the center and surface temperature more accurately compared to the Perzyna model or the hyperbolic sinh model used by Well's et al. [8] (see Figs. 12, 13). The results suggest that accurate determination of the high temperature flow stress is essential for a correct temperature prediction. Another variable influencing the temperature distribution significantly is the friction

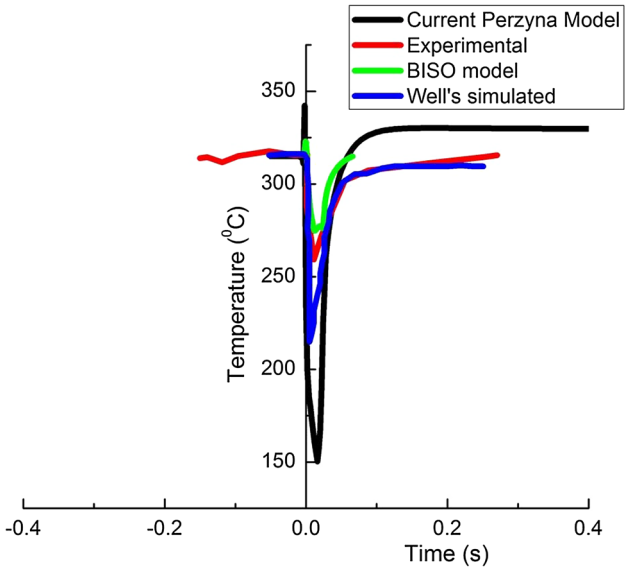

Fig. 12 Variation in the predicted temperature at the strip surface using different models and compared to the experimental results

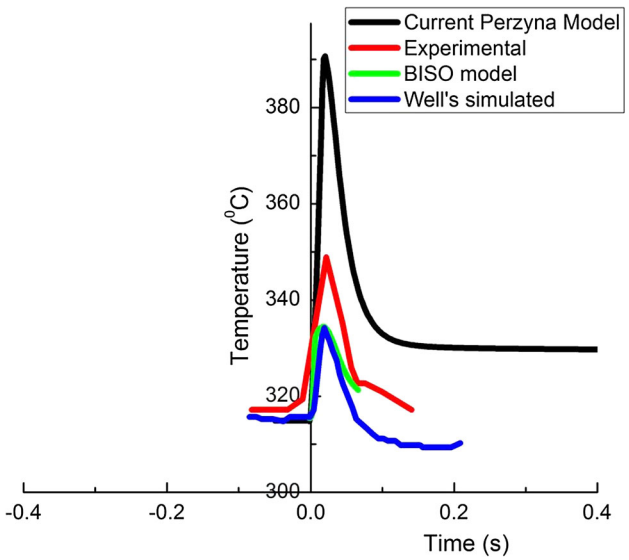

Fig. 13 Variation in the predicted temperature at the strip center using different models compared to the experimental results

coefficient (μ). The actual value of μ depends on factors like roll surface finish, surface oxidation of the workpiece which are unaccounted in this simulation and can affect the temperature predictions.

4.2 Heat Transfer Coefficient and Roll Temperature

Another factor which affects the temperature profile is the temperature at the roll surface and the heat transfer coefficient values used. The discrepancy in choice of heat

transfer coefficient in literature is quite significant. Thus, in the rolling simulation of Al-5 %Mg by Chen et al. [22], a heat transfer coefficient (HTC) of 10–50 kW/m^2 K is used. Most of the published literature uses a HTC value in the above range [12, 16, 17]. However, in the current work this value of HTC fails to simulate the measured experimental temperature drop along the strip surface as it raises the temperature of the strip beyond melting point. Consequently, the HTC along the surface is estimated according to the work of Hlady et al. [43]. In fact, Wells et al. [8] also used the estimates of Hlady et al. [43] for their simulation. Hlady et al. [43] experimentally measured the heat transfer coefficient during hot rolling of AA 5052 and AA 5182 alloys and proposed it to be a function of roll pressure [Eq 10]. According to their work, HTC for these Al alloys are found to vary between 200 and 450 kW/m^2 K. A heat transfer coefficient in the range between 200 and 450 kW/m^2 K reproduces the experimental temperature drop observed in Figs. 12 and 13. However, similar simulation study carried out on an initial plate thickness of 50 mm and percent reduction of 5.74 % uses a HTC value in the range of 10–50 kW/m^2 K [31]. In fact, hot rolling experiments on various steel compositions finds a similar variation in HTC. This work done by Chen et al. [44] observed that the heat transfer coefficient is controlled by rolling parameters like percent reduction, rolling speed, rolling temperature and the alloy type. An increase/decrease in the HTC occurs mainly as a result of the contact pressure during rolling. A high reduction percentage increases the contact pressure which raises the HTC value. For low reduction percent, the contact pressure diminishes, resulting in reduced HTC values.

It may be observed that in the present model, a strip of initial thickness 9.6 mm is reduced by $\sim$20.16 % compared to $\sim$5 % in Duan and Sheppard's work [31]. The higher percent reduction and contact pressure will result in high HTC (in the range 200–450 kW/m^2 K). On the other hand, the lower percent reduction in Ref. [31] favors a decrease in HTC. Another factor affecting HTC is the speed of rolling. At higher rolling speeds, the HTC is high [44]. For the present work, the angular velocity value is 3.5527 radians/second while that obtained from the Duan & Sheppard's experiment is 1.0823 radians/second only. The higher rolling speed in the present work will entail an additional increase in the HTC. Similarly, rolling temperature can also influence heat transfer coefficient. A low rolling temperature causes higher deformation resistance and a higher contact pressure leading to high heat transfer coefficient [44]. Both the present work and the model of Duan & Sheppard [31] have temperature values near to each other. Therefore, the difference in HTC is not on account of any rolling temperature differences.

4.3 Estimate of Coefficient of Friction

As already discussed in Sect. 4.1 the heat generated during rolling depends on both coefficient of friction and the extent of bulk plastic deformation. The value of μ is recalculated using the calculated xy shear stress and pressure obtained from simulation (Eq. 5). The analysis is conducted at three locations, (a) at the entry of strip, (b) middle of the roll-strip interface and (c) at the exit. A coefficient of friction value of 0.48 is obtained at the entry followed by a value of 0.37 at the middle and a value of 0.18 at the exit point. The average coefficient of friction value (0.3) used in the simulation is observed to be in close proximity to the average coefficient of friction for the three points. To further understand the influence of μ on the temperature profile during rolling, the friction coefficient is varied from 0.3 to 0.5 (Figs. 14, 15). A high μ value increases the temperature transient at the strip center while strip surface remains unaffected. The final steady state temperature however increases due to overall increase in heat generation (Figs. 14, 15). The change in μ however results in a slight increase in the strain from the center to the strip surface (Fig. 16).

4.4 Recrystallization During Rolling

As already observed in Fig. 6 the fraction recrystallized during rolling is insignificant. This is on expected lines as for Al–Mg–Mn alloys of the AA 5083 type, particle stimulated DRX is observed at temperatures above 400 °C and at strain rates higher than 1 s^{-1} [17]. Instead a

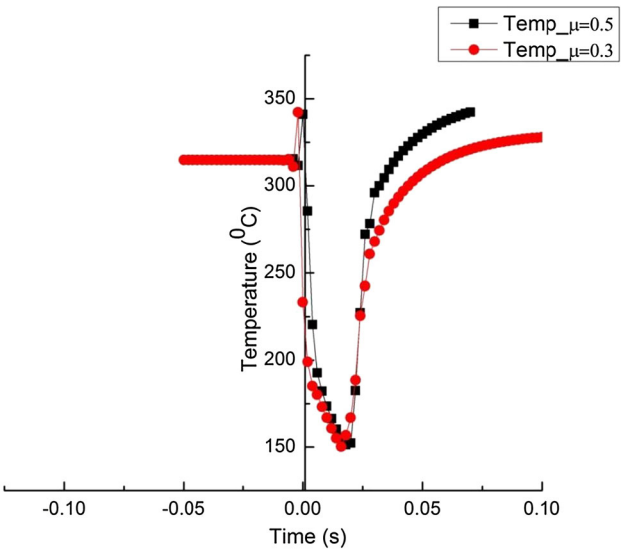

Fig. 14 Temperature profiles at strip surface for different coefficient of friction values of 0.3 and 0.5

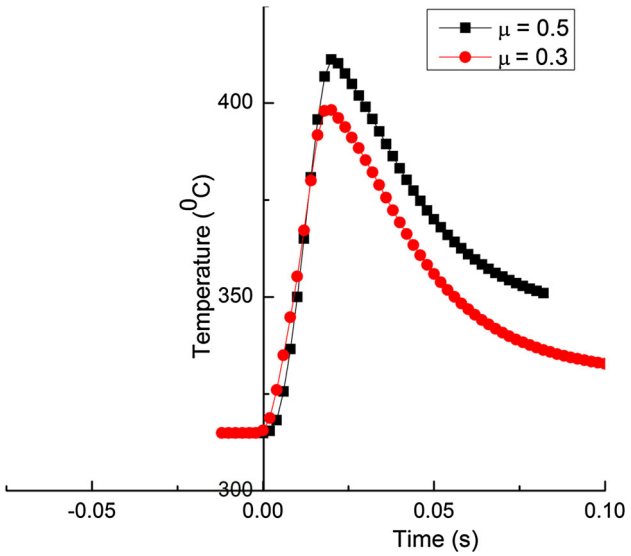

Fig. 15 Temperature profiles at strip center for different coefficient of friction values of 0.3 and 0.5

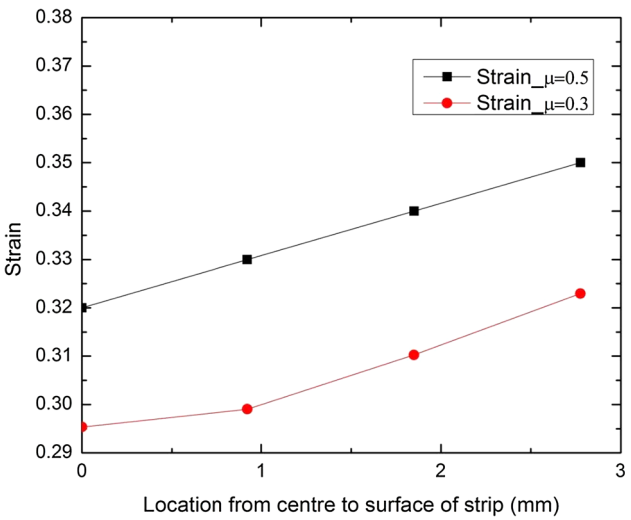

Fig. 16 Strain plots for different coefficient of friction values

significant amount of static recrystallization after rolling is predicted (Fig. 9). For the corresponding experiment by Wells et al. [8], the total post rolling time is 4 s., after which the strip is water quenched to ambient temperature. No actual measurements for the fraction recrystallized is however available for the given experiment [8]. However, recrystallization studies conducted on similar plate thickness and roll diameter at a higher inlet temperature of 397 °C with average strain rate of 11.8 s^{-1} and total strain of 0.28 exhibit fraction recrystallized at the surface as ~20 % at ~2.5 mm from the strip center and between 7 and 10 % near the center. The predicted statically recrystallized fraction at ~2.5 mm is ~10 and ~5 % near the center. The predicted results therefore appears reasonable, considering that the present simulation is for low inlet temperatures (315 °C) and a shorter post rolling period (3 s compared to 8 s). This indicates that the internal variable method in tandem with Avrami equations can predict the microstructure evolution of AA 5083 in a fairly accurate manner.

4.5 Effect of η on Temperature Distribution

Another factor which drastically affects the temperature profile is the value of η i.e. the efficiency of converting deformation energy into heat. In general most of the published literature assumes a value greater than 0.9. However, Hodowany et al. [45] experimentally investigated the partition of plastic work into heat for AA 2024-T3 aluminum alloy and observed that the fraction of plastic work rate converted to heat for plastic strains in the range of 0.2–0.3 lies in the range of 0.4. A reduction in η value from 0.9 to 0.4 results in an accurate peak temperature prediction, although the overall profile differs from the experimental profile (Fig. 17). Although, experimental values of η for AA 5083 alloys is unavailable in literature, variations between different Al alloys is expected. It is to be added that the η value at a given strain can vary with strain rate, although for AA 2024 this sensitivity is observed to be nominal [45].

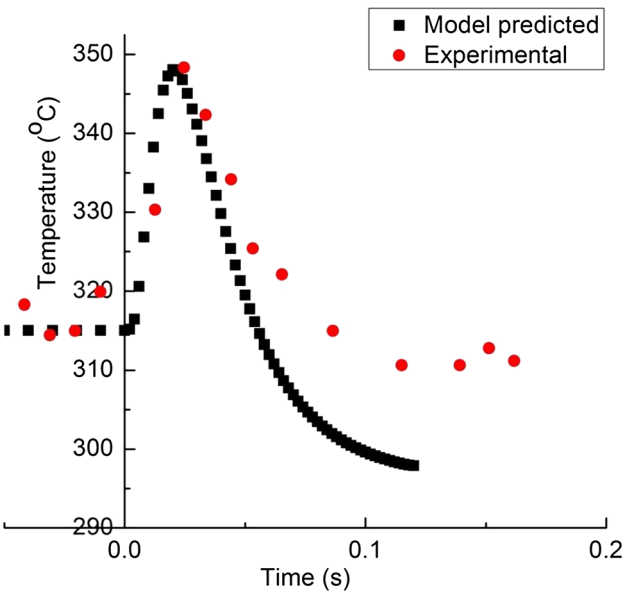

Fig. 17 Temperature profile at the center with heat generated due to plastic deformation for η value of 0.4 compared with experimental plot

5 Conclusions

An integrated thermo-mechanical and microstructure evolution model for hot rolling of a non heat-treatable Al alloy has been developed. The FEM model developed for the thermo-mechanical prediction of the hot rolling process is able to estimate the effect of the temperature and strain and is in overall agreement to experimental results available in literature. The microstructure evolution predictions during static and dynamic recrystallization analysis performed using Avrami and internal variable method fairly agree with the predicted literature results. However, a proper experimental estimate of different process and material parameters plays a vital role in accurate prediction. The effects of some of the process and material parameters on the thermo-mechanical simulation can be summarized as,

(a) The dynamic flow stress estimate from the constitutive equation will significantly influence the temperature profile in the rolled material.
(b) The heat transfer coefficient at roll and material interface depends on the rolling pressure. For the 5XXX series Al alloys studied here, the value varies in the range of 200–450 kW m^{-2} K^{-1}.
(c) Proper estimation of efficiency for the conversion of plastic deformation energy to heat is important particularly at low strain levels.
(d) At low strain levels and low entry strip temperatures used in this model, dynamic recrystallization is expected to be nominal.
(e) The microstructure analysis using JMAK equation shows a variation in fraction recrystallized from 0.09 to 0.26 from the center to surface of the strip. This variation is due to the gradient in strain and temperature from center to surface.

References

1. Oh S-I, and Altan T, *Metal Forming and the Finite-Element Method*, Oxford University Press, Oxford (1989).
2. Zienkiewicz O C, and Taylor R L, *The Finite Element Method, Vol. 1*, McGraw-Hill, London (1989).
3. Hwang S, Joun M S, and Kang Y, *J Manuf Sci Eng*, **115** (1993) 290.
4. Zienkiewicz O, Oñae E, and Heinrich J, *Int J Numer Methods Eng* **17 (10)** (1981) 1497.
5. Alberti N, Cannizzaro L, and Micari F, *CIRP Ann Manuf Technol* **39** (1990) 231.
6. Montmitonnet P, Chenot J L, Bertrand-Corsini C, David C, Lung T, Buessler P, *J Manuf Sci Eng* **114** (1992) 336.
7. Shah R K, Roshan H M D, Sastri V M K, and Padmanabhan K A *Thermomechanical aspects of manufacturing and materials processing*. Hemisphere Publishing Corp., New York, United States (1992).
8. Wells M A, Maijer D M, Jupp S, Lockhart G, Van der Winden M R, *Mater Sci Technol* **19** (2003) 467.
9. Ahmed H, Wells M A, Maijer D M, Howes B ., and Van Der Winden M R, *Mater Sci Eng A* **390** (2005) 278.
10. Gottstein G, *Integral Materials Modeling: Towards Physics-Based Through-Process Models*, Wiley, New York (2007).
11. Hirsch J, *Virtual Fabrication of Aluminum Products: Microstructural Modeling in Industrial Aluminum Production*, Wiley-VCH, Weinheim (2007).
12. Sherstnev P, Melzer C, and Sommitsch C, *Int J Mech Sci* **54** (2012) 12.
13. Pietrzyk M, Kusiak J, Kuziak R, Madej Ł, Szeliga D, and Gołąb R, *Metall Mater Trans A* **45 (13)** (2014) 5835.
14. Bambach M and Seuren S, *J Mater Process Technol* **216** (2015) 95.
15. De Pari L, and Misiolek W Z, *Acta Mater* **56 (20)** (2008) 6174.
16. Shahani A R, Setayeshi S, Nodamaie S A, Asadi M A, and Rezaie S, *J Mater Process Technol* **209** (2009) 1920.
17. McQueen H J, Spigarelli S, Kassner M E, and Evangelista E, *Hot Deformation and Processing of Aluminum alloys*, CRC Press, Boca Raton (2011).
18. Montheillet F, and Jonas J, *ASM Handb* **22** (2009) 220.
19. Sandström R, and Lagneborg R, *Acta Metall* **23** (1975) 387.
20. ANSYS V, *10.0 User's Manual,* ANSYS Inc, Canonsburg (2004).
21. Montmitonnet P, and Buessler P, *ISIJ Int* **31** (1991) 525.
22. Chen B, Thomson P, and Choi S, *J Mater Process Technol* **30** (1992) 115.
23. Timothy S P, Yiu H L, Fine J M, and Ricks R A, *Mater Sci Technol* **7** (1991) 255.
24. Ahmed H, Wells M A, Maijer D M, Lockhart G, and Van der Winden M R, *Metall Mater Trans A* **38** (2007) 922.
25. Pietrzyk M, Cser L, and Lenard J, *Mathematical and Physical Simulation of the Properties of Hot Rolled Products*, Elsevier, Amsterdam (1999).
26. Perzyna P, *Adv Appl Mech* **9** (1966) p 243.
27. Devadas C, Samarasekera I, and Hawbolt E, *Metall Trans A* **22** (1991) 335.
28. Fletcher J, and Beynon J, *Ironmak Steelmak* **23** (1996) 52.
29. Choquet P, Fabregue P, Giusti J, Chamont B, Pezant J N and Blanchet F, *Mathematical Modelling of Hot Rolling of Steel*, CIM, Montreal (1990) p 34.
30. Hlady C O, Brimacombe J K, Samarasekera I V, and Hawbolt E B, *Metall Mater Trans B* **26** (1995) 1019.
31. Duan X, and Sheppard T, *J Mater Process Technol* **150** (2004) 100.
32. Canas J, Picon R, Pariis F, Blazquez A, and Marin J C, *Comput Struct* **58** (1996) 59.
33. Porter D A, Easterling K E, and Sherif M, *Phase Transformations in Metals and Alloys, (Revised Reprint)*, CRC press, Boca Raton (2009).
34. Pietrzyk M, *Metall Foundry Eng (Poland)* **20** (1994) 429.
35. Davies C H, *Scr Metall Mater* **30** (1994) 349.
36. Pietrzyk M, *J Mater Process Technol* **125** (2002) 53.
37. Harlow D, Wei R, and Wang M, *Metall Mater Trans A* **37 (11)** (2006) 3367.
38. Kamikawa N, Huang X, Tsuji N, and Hansen N, *Acta Mater* **57 (14)** (2009) 4198.
39. Rollett A, Humphreys F J, Rohrer G S, and Hatherly M, *Recrystallization and Related Annealing Phenomena*, Elsevier, Amsterdam (2004).
40. Huang Y, and Humphreys F, *Mater Chem Phys* **132** (2012) 166.
41. Hensel A, and Spittel T, *Kraft-und Arbeitsbedarf bildsamer Formgebungsverfahren*, Deutscher Verlag für Grundstoffindustrie Leipzig.
42. Zhou M, and Clode M, *Mech Mater* **27** (1998) 63.

43. Hlady C O, Samarasekera I V, Hawbolt E B, and Brimacombe J K, *Heat Transfer in The Hot Rolling of Aluminium Alloys*, in Proceedings of International Symposium on Light Metals Processing and Applications: 32nd Conference of Metallurgists, Metallurgical Society of CIM Quebec City (1993).
44. Chen W, Samarasekera I, and Hawbolt E, *Metall Trans A*, **24** (1993) 1307.
45. Hodowany J, Ravichandran G, Rosakis A J, and Rosakis P, *Exp Mech* **40** (2000) 113.